Comput. Methods Appl. Mech. Engrg. 268 (2014) 871–883

Contents lists available at ScienceDirect

Comput. Methods Appl. Mech. Engrg.

journal homepage: www.elsevier.com/locate/cma

A multiscale approach for modeling progressive damage of composite materials using fast Fourier transforms

J. Spahn [a,b,*], H. Andrä [a], M. Kabel [a], R. Müller [b]

[a] Fraunhofer Institute for Industrial Mathematics (ITWM), Department Flow and Material Simulation, Fraunhofer-Platz 1, 67663 Kaiserslautern, Germany
[b] Institute of Applied Mechanics, Technische Universität Kaiserslautern, Gottlieb-Daimler-Straße, 67663 Kaiserslautern, Germany

ARTICLE INFO

Article history:
Received 7 June 2013
Received in revised form 25 September 2013
Accepted 8 October 2013
Available online 28 October 2013

Keywords:
Multiscale analysis
Computational homogenization
Continuum damage mechanics
Fast Fourier transforms
Composite materials

ABSTRACT

Composite materials possess a highly complex material behavior, and thus advanced simulation techniques are necessary to compute their mechanical response. In this regard, especially modeling failure and progressive damage presents a challenging task. Conventional macro mechanical methods and even closed form estimates are in many cases not sufficient to predict the appropriate mechanical material response. Full-field simulations must be resorted to, but these are known to be very expensive from the computational point of view. In this contribution we propose a more efficient multiscale approach similar to FE^2. Nonlinear material effects caused by progressive damage behavior are captured directly on the discretized material level using simple isotropic continuum damage laws. In contrast to conventional FE^2 methods which use the Finite Element Method (FEM) to solve both scales numerically, the fine scale problem (material level) is rewritten in an integral form of Lippmann–Schwinger type and solved efficiently using the fast Fourier transformation (FFT). The calculation is carried out on a regular voxel grid that can be obtained from 3D images like tomographies. The fine scale problem is integrated in a standard Finite Element framework which is used to solve the macroscopic BVP (component level). In the work at hand, the scale coupling technique and the computation of the macroscopic tangent are described, and in some numerical examples the convergence behavior of the macroscopic Newton algorithm is investigated. Thereby the simulations were considered until localization and softening on the material scale occurred. It is shown that the proposed method presents an effective way to determine the exact physical macroscopic response considering arbitrary microstructures and loading conditions.

1. Introduction

Besides their outstanding mechanical properties in terms of strength and stiffness related to their weight, fiber-reinforced composite materials possess a highly complex material behavior. In order to use these composite materials efficiently, advanced simulation techniques are necessary. Especially modeling failure and progressive damage of composite materials, presents a major challenge in current research activities. Composite failure occurs as a result of a variety of complex microstructural damage mechanisms, such as matrix damage, fiber pull out and fiber breakage.

Recently, phenomenological macroscale models are state of the art, especially for failure investigations of laminated composite applications, see for instance the work of Maimí et al. [31] or Pinho et al. [44]. These models assume homogeneous

* Corresponding author at: Fraunhofer Institute for Industrial Mathematics (ITWM), Department Flow and Material Simulation, Fraunhofer-Platz 1, 67663 Kaiserslautern, Germany. Tel.: +49 631 31600 4509; fax: +49 631 31600 1099.
E-mail address: spahn@itwm.fraunhofer.de (J. Spahn).
URL: http://www.itwm.fraunhofer.de (J. Spahn).

0045-7825/$ - see front matter © 2013 Elsevier B.V. All rights reserved.
http://dx.doi.org/10.1016/j.cma.2013.10.017

material behavior and are usually based on macroscopic failure criteria, like those proposed by Puck [45] or Cuntze [10]. Disadvantages are the extensive identification of material parameters in dependence of the material structure and the loading conditions. Physical phenomena occurring on a finer length scale are not considered.

A more accurate approach is to capture nonlinear material effects directly on a finer length scale. Recent multiscale modeling and simulation techniques were developed to limit the increasing computational effort to an acceptable extent [25,53]. In this context, analytical methods based on closed form estimates to consider the micro mechanical material structure by means of analytical approximations, represent an efficient and practicable way. Mean field approaches are based on Eshelby's inclusion theory [14] and make use of analytical approximations like the Mori–Tanaka model [39], the double inclusion method [43], or self-consistent schemes [21] to obtain effective material properties. These closed form estimates are restricted to certain inclusion shapes (ellipsoidal, convex, unbent) and are therefore restricted to simple microstructures which are locally uniformly distributed in terms of their size, orientation and volume density. Further the volume fraction of the inclusions is restricted, the stress in the inclusions is assumed to be constant and the interactions between inclusions are only captured to a limited degree, what is an important limitation for the simulation of the evolution of micro cracks. Progressive damage is usually modeled using empirical failure criteria, like e.g. Tsai-Wu, Tsai-Hill, maximum stress or strain criterion, which are based on the work of Tsai and Wu [50] and Hill [22]. An overview of classical analytical methods can be found in [42,43]. Moreover, higher order theories have been proposed using nonlinear extensions of the Hashin–Shtrikman [18] variational principle [5] or the secant/tangent moduli of the phases [6,7]. Furthermore, semi-analytical methods like the Generalized Method of Cells [1] or the Transformation Field analysis (TFA) proposed by Dvorak [13] and extended by e.g. Chaboche et al. [8] or Fish et al. [17] were developed. Moreover in this context, Michel and Suquet [36] introduced the so called nonuniform TFA.

However, to overcome the essential shortcomings related to these kind of models one has to resort to direct or full-field simulations. Therein, the microstructural constituents are modeled explicitly on the interesting scale instead of forming effective constitutive equations. The resulting material response is based on genuine physical effects and consequently arbitrary complex non-proportional, multiaxial loading conditions can be captured. Moreover, simple (isotropic) constitutive laws can be used to define the material behavior of the microstructural constituents and the required parameters can be measured directly in physical experiments. In the last decade, several numerical multiscale modeling and simulation techniques were developed. According to [3,51], these numerical multiscale methods can be divided into concurrent and hierarchical ones. In concurrent methods the scales are strongly coupled and solved simultaneously. The domain is decomposed into a fine- and a coarse-scale model, whereby both scales are linked together "on the fly". Information is mutually exchanged between both scales. On the other hand hierarchical methods pre-compute effective properties from the microscale and pass this information to the uncoupled macroscale. Both scale problems are separated from each other and are solved sequentially. If the assumption of the separation of scales is valid, then the micro problem can be regarded as a representative sample of the microscopic material behavior. One well-known method, which has characteristics of both classes, is the FE^2 approach introduced by Feyel and Chaboche [16] and Smit et al. [48]. The scales are solved separately and every macroscopic point is equipped with a certain microstructure, which describes the material behavior and can be regarded as a representative volume element (RVE). The constitutive equation of the coarse scale is replaced by an associated microscopic boundary value problem (BVP). Information passes in both directions and a mutual exchange between both scales takes place. This class of models can be denoted as semi-concurrent or coupled hierarchical methods.

However, the detailed resolution of the microstructural constituents leads to a fine discretization of the computational model and thus to large algebraic systems with many degrees of freedom. Despite increasing computational power, simulations of macroscopic components using explicitly modeled realistic microstructures can today hardly be realized with reasonable CPU times. Due to the increased computational costs coming along with the application of a multiscale framework, an effective solution of the micro boundary value problem is necessary. In this work an alternative method is applied which uses the fast Fourier transformation (FFT) to solve an equivalent micro BVP (material level). A periodic BVP known from ordinary elasticity problems is reformulated in an integral equation of a so called Lippmann–Schwinger type, as proposed by Zeller and Dederichs [52] and Kröner [27]. The numerical method was introduced by Moulinec and Suquet [40,41,33]. Advantages of this method are its efficiency in terms of memory consumption and computational time. Further the calculation is carried out on a regular voxel grid and could therefore directly be applied to calculate homogenized quantities on 3D images like tomographies without using any complicated mesh generation. The fine scale problem can easily be integrated in a standard Finite Element framework which is used to solve the macroscopic BVP (component level).

In the first part of this paper, the constitutive equation and the numerical solution of the microscale model are introduced and demonstrated by an illustrative numerical example. The second part presents the coupling technique of the two geometrical scales by combining the two numerical methods. The numerical homogenization process including the computation of the macroscopic tangent by using the FFT method are explained. Finally, the paper closes with numerical examples of some scale coupling problems to illustrate the macroscopic convergence behavior of the numerical method. The examples shown in this work were considered until material softening appeared. This means the simulations were stopped when localization on the material scale occurred, so that the governing equation keep its ellipticity and the assumption of separation of scales remains valid.[1]

[1] In the opinion of the authors this should be satisfactory in this case, due to the brittle fracture characteristics of the considered fiber reinforced composite materials.

2. Microscale model

2.1. Continuum damage mechanics formulation

In this work we use a simple strain based continuum damage model according to Simo and Ju [47] to describe the matrix fracture, whereby any other constitutive model can be used to describe the material behavior of the microscopic constituents.

In the context of continuum damage mechanics (CDM), Kachanov [24] introduced an internal variable d ranging from 0 to 1. While $d = 0$ represents the undamaged state, $d = 1$ describes the status of completely failed material. The constitutive equation is derived from a thermodynamic state potential, the Helmholtz free energy

$$\psi = \frac{1}{2}(1-d)\ \boldsymbol{\varepsilon} : \mathbb{C}_{\mathrm{el}} : \boldsymbol{\varepsilon}. \tag{1}$$

The cauchy stress is defined by:

$$\boldsymbol{\sigma} = \frac{\partial \psi}{\partial \boldsymbol{\varepsilon}} = (1-d)\ \mathbb{C}_{\mathrm{el}} : \boldsymbol{\varepsilon}, \tag{2}$$

where $\mathbb{C}_{\mathrm{el}}$ is the isotropic elasticity tensor. The specific strain energy is the thermodynamic force Y associated with the internal state variable d

$$Y = -\frac{\partial \psi}{\partial d} = \frac{1}{2}\ \boldsymbol{\varepsilon} : \mathbb{C}_{\mathrm{el}} : \boldsymbol{\varepsilon}. \tag{3}$$

For the isothermal case the second law of thermodynamics can be expressed in terms of the Clausius–Duhem inequality $\mathcal{D} = \mathcal{P} - \dot{\psi} \geqslant 0$. With the rate of mechanical work $\mathcal{P} = \boldsymbol{\sigma} : \dot{\boldsymbol{\varepsilon}}$ and the absence of further dissipative processes one obtains the Clausius–Duhem inequality in the following form:

$$\mathcal{D} = Y\dot{d}\ \geqslant\ 0. \tag{4}$$

A damage criterion f controls the state of damage, which is in the case of growing damage described by a monotonic function $\phi(Y)$

$$f(Y,d) = \phi(Y) - d \leqslant 0 \quad \begin{cases} f < 0 & \text{elastic}, \\ f = 0 & \text{damage}. \end{cases} \tag{5}$$

The above damage criterion function f and the dissipation inequality (4) in combination with the principle of maximum dissipation leads according to [47,28] to a constrained optimization problem

$$\mathcal{L} = -\mathcal{D} + \dot{\lambda} f = -Y\dot{d} + \dot{\lambda}(\phi(Y) - d). \tag{6}$$

Thereby the Lagrangian multiplier $\dot{\lambda} \geqslant 0$ is introduced and $\mathcal{D}$ has to be maximized subject to the constraint $f = 0$. The solution of the Lagrangian functional leads to an evolution law for the damage variable d

$$\dot{d} = \frac{\partial f}{\partial Y}\dot{\lambda} = \frac{\partial \phi}{\partial Y}\dot{\lambda} \quad (\text{for } f = 0). \tag{7}$$

Introducing the loading/unloading conditions according to the Kuhn–Tucker relations here with $\dot{\lambda}$ as the damage consistency parameter

$$f \leqslant 0, \quad \dot{\lambda} \geqslant 0, \quad f\dot{\lambda} = 0 \tag{8}$$

and assuming that $\phi(\cdot)$ is a monotonic increasing function $\dot{\lambda}$ is determined by the consistency condition

$$\dot{f} = f = 0 \quad \Rightarrow \quad \dot{\lambda} = \dot{Y}. \tag{9}$$

This results in a closed form expression for the damage variable

$$\dot{d} = \frac{\partial \phi(Y)}{\partial Y}\dot{Y} = \dot{\phi}(Y) \quad \Rightarrow \quad d = \phi(Y) + d_0. \tag{10}$$

In the work at hand the initial damage value $d_0 = 0$ and the following functional form for the growing damage variable d is chosen:

$$\phi(Y) = 1 - \mathrm{e}^{(-H(\tilde{\varepsilon}_{(Y)} - Y_0))}, \quad d \in [0,1), \tag{11}$$

$$d(t) = \max_{-\infty < \tau < t} \{d(\tau), \phi(Y)\}. \tag{12}$$

In the equation above the material parameters H as the damage hardening modulus and Y_0 as the initial damage threshold are introduced. According to Simo and Ju [47] the strain energy Y is replaced by an equivalent strain measurement $\tilde{\varepsilon}(Y)$ which is obtained by a small modification of Y, namely the energy norm of the strain tensor

$$\tilde{\varepsilon}(Y) = \sqrt{2Y} = \sqrt{\boldsymbol{\varepsilon} : \mathbb{C} : \boldsymbol{\varepsilon}}. \tag{13}$$

There exist several proposals to calculate the equivalent strain (see e.g. [29,32]). Choosing the energy norm of the strain tensor as an equivalent strain measurement in conjunction with the thermodynamic consistent (associated) damage formulation ensures the symmetry of the forth order elastic-damage tangential material modulus $\mathbb{C}^{\text{ed}}_{\text{tan}}$ [47] which relates the stress rate tensor and the strain rate tensor $\dot{\boldsymbol{\sigma}} = \mathbb{C}^{\text{ed}}_{\text{tan}} : \dot{\boldsymbol{\varepsilon}}$

$$\mathbb{C}^{\text{ed}}_{\text{tan}} = (1-d)\mathbb{C}^{\text{el}} - \frac{H}{Y} \mathrm{e}^{-H(Y-Y_0)}\, \boldsymbol{\sigma}^{\text{el}} \otimes \boldsymbol{\sigma}^{\text{el}}. \tag{14}$$

Thereby $\mathbb{C}^{\text{el}}$ denotes the constant elasticity modulus and $\boldsymbol{\sigma}^{\text{el}} = \mathbb{C}^{\text{el}} : \boldsymbol{\varepsilon}$ the elastic (undamaged) stress. Moreover, the elastic-damage secant modulus which relates the stress with the strain tensor $\boldsymbol{\sigma} = \mathbb{C}^{\text{ed}}_{\text{sec}} : \boldsymbol{\varepsilon}$ is described by:

$$\mathbb{C}^{\text{ed}}_{\text{sec}} = (1-d)\mathbb{C}^{\text{el}}. \tag{15}$$

2.2. Equivalent BVP and FFT-based numerical solution

For computing effective quantities of a periodic medium with local stiffness $\mathbb{C}(\boldsymbol{x})$ in the context of a numerical homogenization process, a cubic RVE $\omega \in \mathbb{R}^3$ with periodic boundary conditions on $\partial\omega$ is considered. The local strain field is split into a prescribed constant macroscopic strain $\boldsymbol{E}$ and a fluctuation term $\boldsymbol{\varepsilon}(\boldsymbol{u}^*(\boldsymbol{x}))$.

$$\operatorname{div}\boldsymbol{\sigma}(\boldsymbol{x}) = \boldsymbol{0} \qquad \boldsymbol{x} \text{ on } \omega, \tag{16a}$$
$$\boldsymbol{\sigma}(\boldsymbol{x}) = (1-d(\boldsymbol{x}))\mathbb{C}(\boldsymbol{x}) : \boldsymbol{\varepsilon}(\boldsymbol{x}) \qquad \boldsymbol{x} \text{ on } \omega, \tag{16b}$$
$$\boldsymbol{\varepsilon}(\boldsymbol{x}) = \boldsymbol{E} + \frac{1}{2}\left(\nabla \boldsymbol{u}^*(\boldsymbol{x}) + (\nabla \boldsymbol{u}^*(\boldsymbol{x}))^T\right) \qquad \boldsymbol{x} \text{ on } \omega, \tag{16c}$$
$$\boldsymbol{u}^*(\boldsymbol{x}) \quad \text{periodic} \qquad \boldsymbol{x} \text{ on } \partial\omega_D, \tag{16d}$$
$$\boldsymbol{\sigma}(\boldsymbol{x}) \cdot \boldsymbol{n}(\boldsymbol{x}) \quad \text{anti-periodic} \qquad \boldsymbol{x} \text{ on } \partial\omega_N. \tag{16e}$$

According to Zeller and Dederichs [52] the differential Eq. (16a) can be reformulated in an integral equation, the so called Lippmann–Schwinger equation, which is attributed to Lippmann and Schwinger [30] in the field of quantum mechanics. By introducing a homogeneous reference material with the stiffness $\mathbb{C}^0$, the polarization stress $\boldsymbol{\tau}$ with respect to this reference material and the resulting constitutive equation read as follows:

$$\boldsymbol{\tau}(\boldsymbol{x}) = (1-d(\boldsymbol{x}))\mathbb{C}(\boldsymbol{x}) : \boldsymbol{\varepsilon}(\boldsymbol{x}) - \mathbb{C}^0 : \boldsymbol{\varepsilon}(\boldsymbol{x}), \tag{17}$$

$$\boldsymbol{\sigma}(\boldsymbol{x}) = \mathbb{C}^0 : \boldsymbol{\varepsilon}(\boldsymbol{x}) + \boldsymbol{\tau}(\boldsymbol{x}). \tag{18}$$

The solution of the local problem in Eq. (16) can now be obtained using a nonlocal Green operator $\boldsymbol{\Gamma}^0$ which is applied on the stress polarization $\boldsymbol{\tau}$

$$\boldsymbol{\varepsilon}(\boldsymbol{x}) = \boldsymbol{E} - \left(\boldsymbol{\Gamma}^0 * \boldsymbol{\tau}\right)(\boldsymbol{x}). \tag{19}$$

The operator $\boldsymbol{\Gamma}^0$ is only associated with the stiffness of the homogenous linear elastic reference material $\mathbb{C}^0$ and the given boundary conditions, but does not depend on the fluctuating quantities [27]. The convolution (denoted by '$*$') in Eq. (19) is defined by:

$$\left(\boldsymbol{\Gamma}^0 * \boldsymbol{\tau}\right)(\boldsymbol{x}) = \int_{\omega} \boldsymbol{\Gamma}^0(\boldsymbol{x}-\boldsymbol{y}) : \boldsymbol{\tau}(\boldsymbol{y}) \mathrm{d}\boldsymbol{y}. \tag{20}$$

In the Fourier space it transforms into a direct product and the corresponding relation reads:

$$\hat{\boldsymbol{\varepsilon}}(\boldsymbol{\xi}) = -\hat{\boldsymbol{\Gamma}}^0(\boldsymbol{\xi}) : \hat{\boldsymbol{\tau}}(\boldsymbol{\xi}), \quad \forall \boldsymbol{\xi} \neq \boldsymbol{0},\ \hat{\boldsymbol{\varepsilon}}(\boldsymbol{0}) = \boldsymbol{E}, \tag{21}$$

where $\hat{f}(\cdot)$ denotes a function in the Fourier space and $\boldsymbol{\xi}$ the Fourier space variable corresponding to the coordinates $\boldsymbol{x}$.

$\boldsymbol{\Gamma}^0$ is only associated with the stiffness of the homogenous linear elastic reference material $\mathbb{C}^0$ and the given boundary conditions, but does not depend on the fluctuating quantities [27]. For an isotropic reference material with the Lamé constants λ^0 and μ^0 the Fourier transform of the Green operator $\hat{\boldsymbol{\Gamma}}^0$ is explicitly known [41] and takes the form:

$$\hat{\Gamma}^0_{ijkl}(\xi) = \frac{1}{4\mu^0|\xi|^2}\left(\delta_{ki}\xi_l\xi_j + \delta_{li}\xi_k\xi_j + \delta_{kj}\xi_l\xi_i + \delta_{lj}\xi_k\xi_i\right) - \frac{\lambda^0+\mu^0}{\mu^0(\lambda^0+2\mu^0)}\frac{\xi_i\xi_j\xi_k\xi_l}{|\xi|^4}. \tag{22}$$

Substituting the expression of $\boldsymbol{\tau}$ (17) in (19) we arrive at a nonlinear Lippmann–Schwinger equation:

$$\boldsymbol{\varepsilon}(\boldsymbol{x}) = \boldsymbol{E} - \left(\boldsymbol{\Gamma}^0 * (((1-d)\mathbb{C} - \mathbb{C}^0) : \varepsilon)\right)(\boldsymbol{x}). \tag{23}$$

There exist different numerical schemes to solve the Lippmann–Schwinger integral equation iteratively. In this work the so called basic scheme is used, which was introduced by Moulinec and Suquet [41]. The benefit of the scheme is based on the fact that the constitutive equation is solved in the real space and the convolution integral in the Fourier space. The transformation of the calculated fields is performed by a discrete fast Fourier transformation (FFT). This transformation strongly affects the efficiency of the numerical scheme. Each iteration consists of four steps:

1. Solve the constitutive equation in the real space
2. Fourier transformation of the stress polarization field
3. Convolution with the Green operator in the Fourier space
4. Inverse Fourier transformation of the updated strain field

$$\boxed{\begin{aligned} &\boldsymbol{\tau}^i = \left((1-d^i)\mathbb{C} - \mathbb{C}^0\right) : \boldsymbol{\varepsilon}^i, \\ &\hat{\boldsymbol{\tau}}^i = \mathrm{FFT}(\boldsymbol{\tau}^i), \\ &\hat{\boldsymbol{\varepsilon}}^{i+1} = -\hat{\boldsymbol{\Gamma}}^0 : \hat{\boldsymbol{\tau}}^i, \quad \hat{\boldsymbol{\varepsilon}}^{i+1}(0) = \boldsymbol{E}, \\ &\boldsymbol{\varepsilon}^{i+1} = \mathrm{FFT}^{-1}(\hat{\boldsymbol{\varepsilon}}^{i+1}), \end{aligned}} \tag{24}$$

where $d^i(t)$ is obtained according to Eqs. (11)–(13). The scheme is formulated in terms of the elastic damage law described in Section (2.1), whereby the basic scheme in its general form is applicable for any arbitrary nonlinear constitutive law.

According to [41] convergence is reached when the global stress field is in equilibrium

$$\frac{\left\|\mathrm{div}\boldsymbol{\sigma}^{i+1}\right\|^2}{\left\|\boldsymbol{\sigma}^{i+1}\right\|^2} \leqslant \mathrm{tol}_1, \tag{25}$$

which can easily be computed in the Fourier space:

$$\frac{\left\|\boldsymbol{\xi}\cdot\hat{\boldsymbol{\sigma}}^{i+1}(\boldsymbol{\xi})\right\|^2}{\left\|\hat{\boldsymbol{\sigma}}^{i+1}(\boldsymbol{0})\right\|^2} \leqslant \mathrm{tol}_1. \tag{26}$$

Thereby $\hat{\boldsymbol{\sigma}}(\boldsymbol{0})$ represents the average or macroscopic stress and $\|\cdot\|^2$ denotes the L^2 norm of the appropriate field variable.

In this work a second convergence criterion is applied, which controls the difference of the strain field between two iterations in real space (see e.g. [4]):

$$\frac{\left\|\boldsymbol{\varepsilon}^{i+1} - \boldsymbol{\varepsilon}^i\right\|^2}{\left\|\boldsymbol{E}\right\|^2} \leqslant \mathrm{tol}_2. \tag{27}$$

Typical values for the convergence tolerances are $\mathrm{tol}_1 = 10^{-4}$ and $\mathrm{tol}_2 = 10^{-10}$.

The elastic parameters of the reference material $\mathbb{C}^0$, which have important influence on the convergence rate of the scheme, are chosen according to [41]:

$$k^0 = \frac{1}{2}\left(\min_x k(x) + \max_x k(x)\right), \quad \mu^0 = \frac{1}{2}\left(\min_x \mu(x) + \max_x \mu(x)\right), \tag{28}$$

where μ and k denote shear and bulk modulus of an isotropic material.

The convergence rate generally depends on the stiffness contrast of the material phases. In particular, progressive damage behavior leads to higher stiffness contrasts and consequently the convergence behavior becomes worse. In this context it should be mentioned that in the last decade certain numerical schemes were developed to improve the convergence behavior of the FFT method for materials with high stiffness contrasts. First the augmented Lagrangian scheme was established to improve the convergence of the basic scheme for composites with high contrasts [34,35]. Moreover, in this context, the accelerated scheme was introduced by Eyre and Milton [15] for electrical conductivity problems. The most promising scheme applicable to arbitrary phase contrasts was derived by Brisard and Dormieux [4] within a variational framework from the upper Hashin-Shrikman [18] bound. A review of different schemes and an analysis of the convergence behavior for the computation of precise bounds of effective properties in comparison with analytical estimates can be found in [23].

2.3. Example convergence microscale model

In the following example the convergence behavior of the microscopic model is illustrated. The cubic microstructure contains an elastic spherical inclusion and is discretized by 8000 voxel cells. The behavior of the inclusion is assumed to be linear elastic, while for the polymer matrix the isotropic damage model described in Section (2.1) is used. The structure is loaded with periodic deformation BCs and solved numerically with the FFT scheme described in the section above. In a nonlinear

load step the two different convergence criteria according to Eqs. (26) and (27) are investigated. Further a third criterion is demonstrated, which is calculated by the difference between the norm of the strain fields of two iterations

$$\frac{\left|\left\|\boldsymbol{\varepsilon}^{i+1}\right\|^2 - \left\|\boldsymbol{\varepsilon}^{i}\right\|^2\right|}{\left\|\boldsymbol{E}\right\|^2} \leqslant \text{tol}. \tag{29}$$

This criterion is very effective in terms of memory consumption, because only the norm of the strain field has to be stored in each iteration instead of the entire field of the solution. As illustrated in Fig. 1 the two conventional criteria behave very stable, while the strain error (Eq. (27)) decreases faster than the error of the equilibrated stress field (Eq. (26)). For that reason the typical tolerance value of 10^{-10} is much smaller in comparison to 10^{-4} for error of the stress field. The memory optimized criterion seems to be unstable in some areas and has to be used with caution.

3. Multiscale approach

3.1. Model description

For the investigation of the macroscopic damage behavior the microscopic model is extended to a multiscale framework. Therefore the two scales are related to each other by a procedure similar to the FE^2 approach [16,48]. Thus the constitutive equation on the macroscale is replaced by a BVP on the microscale (see Fig. 2).

Each macroscopic point is linked to a RVE which represents the particular microstructure at this point. The variables which are transferred between both scales are defined by volume averages $\langle\cdot\rangle = \frac{1}{\omega}\int_\omega(\cdot)\,d\omega$ over the micro domain

$$\boldsymbol{E} = \langle\boldsymbol{\varepsilon}\rangle, \quad \boldsymbol{\Sigma} = \langle\boldsymbol{\sigma}\rangle, \quad D = \langle d\rangle. \tag{30}$$

The computation of the macroscopic stress during the homogenization procedure has to meet the energy criterion proposed by Hill [20] or more precise, the micro–macro work balance in differential form must be satisfied

$$\boldsymbol{\Sigma} : \dot{\boldsymbol{E}} = \langle\boldsymbol{\sigma} : \dot{\boldsymbol{\varepsilon}}\rangle. \tag{31}$$

The criterion states that the rate of mechanical work done at the microscale equals the rate of work resulting from the computed macroscopic quantities. This isn't valid for all kind of BCs applied to the RVE. In this work strain-controlled periodic BCs according to Eq. (21) are applied on the microscopic BVP, which is defined in Eq. (16).

On the macroscale mixed BCs could be used and hence the macroscopic BVP reads as follows:

$$\operatorname{div}\boldsymbol{\Sigma}(\boldsymbol{x}) = \boldsymbol{0} \qquad \boldsymbol{x} \text{ on } \Omega, \tag{32a}$$

$$\boldsymbol{E}(\boldsymbol{x}) = \frac{1}{2}\left(\nabla\boldsymbol{U}(\boldsymbol{x}) + \nabla^T\boldsymbol{U}(\boldsymbol{x})\right) \qquad \boldsymbol{x} \text{ on } \Omega, \tag{32b}$$

$$\boldsymbol{U}(\boldsymbol{x}) = \boldsymbol{U}_0(\boldsymbol{x}) \qquad \boldsymbol{x} \text{ on } \partial\Omega_D, \tag{32c}$$

$$\boldsymbol{\Sigma}(\boldsymbol{x}) \cdot \boldsymbol{N}(\boldsymbol{x}) = \boldsymbol{T}_0(\boldsymbol{x}) \qquad \boldsymbol{x} \text{ on } \partial\Omega_N, \tag{32d}$$

where $\boldsymbol{U_0}(\boldsymbol{x})$ and $\boldsymbol{T_0}(\boldsymbol{x})$ denote the prescribed macroscopic displacement vector and surface force vector on the Dirichlet and Neumann boundary of the macroscopic domain Ω.

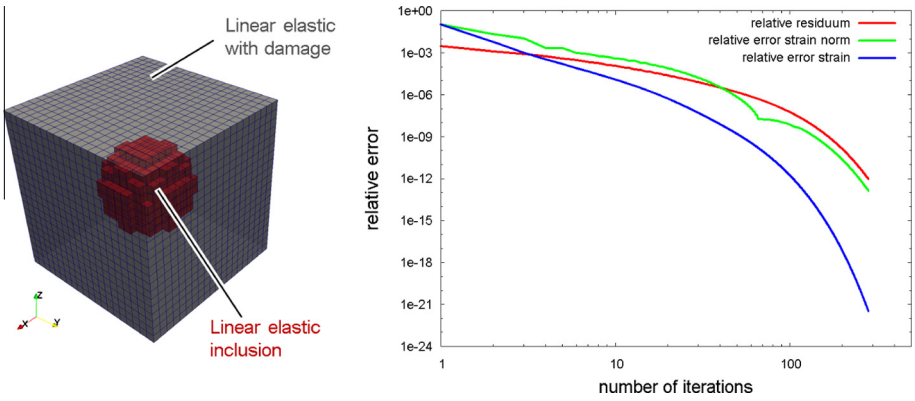

Fig. 1. Microscopic setup (left) and relative error of the microscopic inclusion problem over the number of FFT iterations for a single nonlinear load step (right).

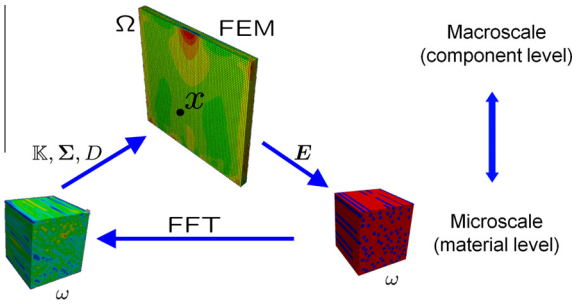

Fig. 2. Scale coupling and multiscale approach schematically.

The macroscopic BVP is solved using a standard Newton–Raphson scheme. Hence, in each macroscopic Newton iteration the averaged microscopic stresses $\langle \boldsymbol{\sigma} \rangle$ have to be computed for setting up the macroscopic residual force vector. Additionally, for an efficient macro computation, the macroscopic tangential stiffness $\mathbb{K}$ is required. It is defined by the following derivative:

$$\mathbb{K} = \frac{\partial \boldsymbol{\Sigma}}{\partial \boldsymbol{E}}. \tag{33}$$

The macroscopic tangent can be directly obtained by using the condensed microscopic (global) stiffness matrix received from the RVE computation as proposed by Kouznetsova et al. [26]. Thereby the macroscopic stress $\boldsymbol{\Sigma}$ is computed by averaging the RVE stresses $\boldsymbol{\sigma}$ over the whole micro domain. Miehe and Koch [38] proposed a more efficient way to compute the macroscopic quantities considering only the RVEs boundary.

The direct tangent computation appears from the numerical point of view very efficient, but at the same time, the requirement of a Schur complement computation is associated with high memory allocation. In this work, we compute the macroscopic tangent by numerical linearization around the current macroscopic load step. This is done by applying six infinitesimally deformation states on the equilibrated stress field. By adding a small perturbation strain $\delta \boldsymbol{E}$ on the equilibrated strain field which was computed during the current macroscopic load step, the numerical tangent is calculated by the following equation:

$$\delta \boldsymbol{\Sigma} = \mathbb{K}_{\delta E} : \delta \boldsymbol{E}, \tag{34}$$

where $\delta \boldsymbol{\Sigma}$ denotes the perturbation of the macroscopic stress caused by $\delta \boldsymbol{E}$. For an infinitesimal small $\delta \boldsymbol{E}$ the numerical tangent equals the analytical one which is defined in Eq. (33)

$$\lim_{\delta E \to 0} \mathbb{K}_{\delta E} = \mathbb{K}. \tag{35}$$

But the perturbation must not be too small, to avoid numerical problems. In this context some authors investigated the size of the perturbation in dependence of the existing machine precision (see, [12,37]). In literature values between 10^{-8} and 10^{-6} are mostly proposed to obtain an efficient macroscopic convergence behavior. In this work $\|\delta \boldsymbol{E}\| = 10^{-6}$ yield sufficiently accurate results.

The computation of the perturbation load cases requires additional computational time, but the Schur complement computation coming along with memory expensive matrix inverting is avoided. Thus, larger micro systems can be treated.

For an efficient macroscopic Newton algorithm the macroscopic tangent obtained by the perturbation procedure has to be consistent with the macroscopic stress which is computed during the macroscopic load step. Hence, the boundary conditions applied on the RVE for the computation of both macroscopic quantities have to be compatible with each other. Moreover, the evolution of the internal variables during the perturbation step has to be consistent with the macroscopic load step. Dealing with internal variables on the microscale different techniques can be used to obtain a consistent macroscopic tangent during the perturbation step, see [49] for a detailed study.

Performing the perturbation step with frozen internal variables leads to an elastic secant stiffness. To obtain a consistent tangent stiffness the internal variables have to be able to evolve during the perturbation step. The authors of [49] proposed the evolution of the internal variables under certain constraint conditions. In dependence of the local damage evolution history during the current load step Δt^{n+1} a particular material point of the RVE behaves elastically or inelastically during the perturbation step. Miehe [37] proposed an alternative approach for obtaining the consistent tangent stiffness by loading back from the last load step. In this work, the perturbation is done by applying the current macro load in addition with the particular perturbation strain. The internal variables evolve inelastic and unconstrained, i.e. independent form the current load history. The solution field obtained at the end of the current load step Δt^{n+1} is stored and reloaded in each perturbation load case, while the internal variables are stored at the beginning of the next macroscopic load step.

After the macroscopic load step Δt^{n+1} is solved, the microscopic stresses and the internal variables are obtained from the constitutive equation. Volume averaging over the whole micro domain gives the macroscopic stress

$$\boldsymbol{E}^{n+1} = \boldsymbol{E}^{n} + \Delta\boldsymbol{E}^{n+1}, \tag{36}$$

$$\boldsymbol{\sigma}^{n+1} = \boldsymbol{\sigma}\left(\boldsymbol{E}^{n+1}, d^{n+1}\right), \tag{37}$$

$$\boldsymbol{\Sigma}^{n+1} = \frac{1}{\omega}\int_{\omega} \boldsymbol{\sigma}^{n+1}\, d\omega. \tag{38}$$

For the computation of the macroscopic tangent according to Eq. (34) the perturbations of the macroscopic stress are required

$$\delta\boldsymbol{\Sigma}^{n+1} = \boldsymbol{\Sigma}\left(\boldsymbol{E}^{n+1} + \delta\boldsymbol{E},\ d^{n} + \delta d(\Delta\boldsymbol{E}^{n+1} + \delta\boldsymbol{E})\right) - \boldsymbol{\Sigma}\left(\boldsymbol{E}^{n+1}, d^{n+1}\right). \tag{39}$$

3.2. Onset of macroscopic failure

In some cases, e.g. in the case of softening material behavior, the assumption of the separation of scales is no longer valid. Microscopic failure leads to the loss of ellipticity of the governing differential equation and consequently the problem becomes ill-posed [46,19]. Occurring localized micro cracks lead to evolving macro cracks and special scale coupling techniques are necessary to describe failure evolution on the coarse scale. For instance, Belytschko et al. [2] proposed a method, called multiscale aggregating discontinuities, which allows to transport a discontinuity between the scales. The latter is injected at the macroscale by the extended finite element method. Coenen et al. [9] established a special multiscale framework which enables the incorporation of a shear band into the microstructural sample and an effective displacement jump is transported to the macroscale (see also Linder [54,55]). The failed micro material sample is not any more representative for the whole micro structural behavior and consequently it is denoted as microstructural volume element, MVE. This work is only related to pre-failure material behavior i.e. the state before localization of the macroscale occurs and consequently the separation of scales remains valid. The micro samples can be regarded as RVEs.

The point when the problem becomes ill-posed can be regarded as the onset of macroscopic failure. It is detected by an analysis of the acoustic tensor of the current homogenized tangent stiffness tensor [19,46]. The acoustic tensor $\boldsymbol{A}(\boldsymbol{n})$ is calculated by the macroscopic tangent stiffness $\mathbb{K}$ and all possible orientations $\boldsymbol{n}$ [11]

$$A_{jk}(n) = K_{ijkl} n_i n_l, \tag{40}$$

$$\boldsymbol{n} = \boldsymbol{n}(\varphi, \theta), \tag{41}$$

$$\|\boldsymbol{n}\| = 1, \tag{42}$$

where the definition of the acoustic tensor $\boldsymbol{A}$ is given in index notation. The orientations $\boldsymbol{n}$ can be expressed by two angles (φ and θ). Localization occurs, if the following criterion is fulfilled for a certain direction $\boldsymbol{n}$:

$$\det\left(\boldsymbol{A}(\boldsymbol{n})\right) = 0. \tag{43}$$

We demonstrate this analysis on a cubic RVE containing a single linear elastic fiber inclusion (see Fig. 3). The structure is discretized by 75^3 (421,875) voxel cells and loaded during 10 time steps with a uniaxial macroscopic strain perpendicular to the fiber direction.

In each time step the homogenized macroscopic tangent is computed with the perturbation procedure. Subsequently, the acoustic tensor determinant is calculated for all directions.

In Fig. 4 the normalized determinant of the acoustic tensor is plotted in all directions using spherical coordinates. Thereby the value of the determinant illustrated as the spherical radius decreases with growing damage in the direction which is perpendicular to the crack direction.

4. Numerical examples

4.1. Multiscale simulation spherical inclusion

In Fig. 5 an example for a fully coupled multiscale approach is demonstrated. A strip with a hole modeled with 516 tetrahedral finite elements is coupled to the RVE structure which was already used in Section 2.3 discretized by 20^3 (8000) voxel cells. All macroscopic integration points are fully coupled with the same RVE. The matrix material of the RVE is modeled by the isotropic damage model described in Section 2.1 and the behavior of the inclusion is assumed to be linear elastic.

Growing damage on the fine scale with an increasing macroscopic load results in macroscopic reduction of stiffness. Consequently, the macroscopic stress–strain response shows a nonlinear material behavior. The damage distribution of the macroscale and the stress–strain response is illustrated in Fig. 6.

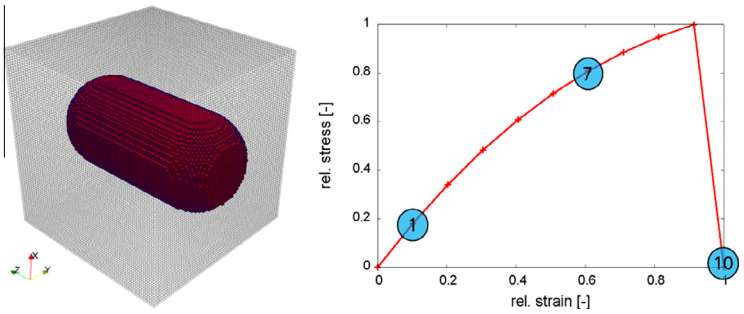

Fig. 3. Unit cell containing a single elastic fiber (left) and normalized stress–strain plot of the failed structure (right).

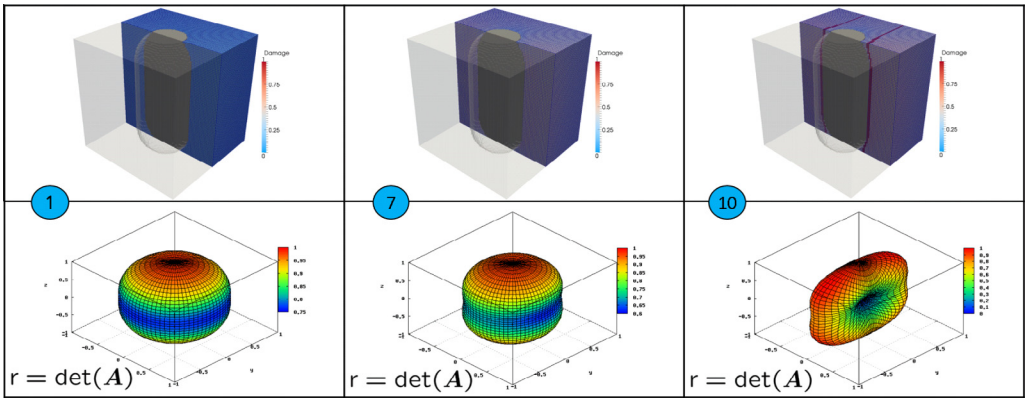

Fig. 4. Detection of the onset of macroscopic failure with the acoustic tensor.

In Fig. 7 the convergence behavior of the macroscopic Newton algorithm is illustrated over the load step history. On the left the relative residuum is plotted against the total number of macro Newton iterations. As a second measure of the macroscopic error the norm of the update of the solution relative to the norm of the solution, i.e. $\|\Delta \boldsymbol{U}\|/\|\boldsymbol{U}\|$ is shown.

Quadratic convergence is observed for all load steps. The CPU time of the entire problem was around 13 h on a standard workstation, while a single RVE computation took only a few seconds. For this and the following simulations illustrated in this work, a convergence criterion by means of the relative error of the solution $\boldsymbol{U}$ of 10^{-6} was chosen.

4.2. Multiscale simulation fiber composite

In Fig. 8 an example for a fully coupled multiscale approach with a more realistic micro structure is demonstrated. The strip with a hole discretized by 516 tetrahedral finite elements is coupled to short fiber reinforced RVE structures which are modeled with 64^3 (262,144) voxel cells. RVEs with 45° fiber orientation with respect to the macro loading direction are associated to the macroscopic integration points. However, for each different macroscopic point any arbitrary RVE structure

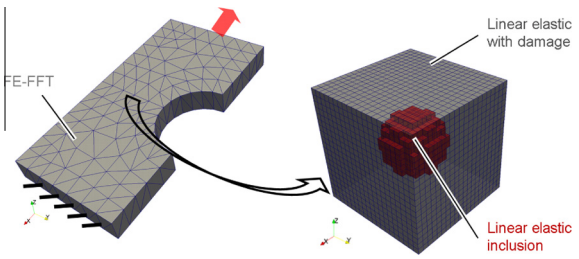

Fig. 5. Multiscale simulation strip with a hole (macro) and a cubic RVE containing a single spherical inclusion (microscale).

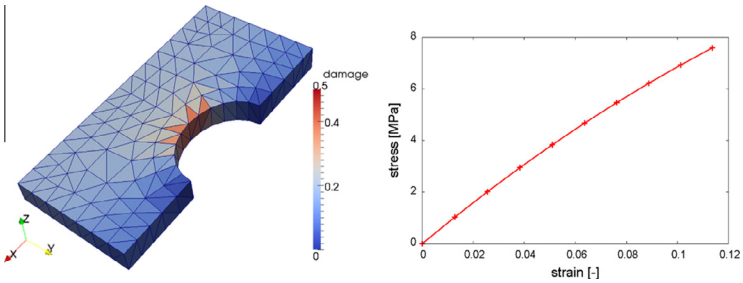

Fig. 6. Damage distribution (left) and stress–strain response (right) of the macroscale.

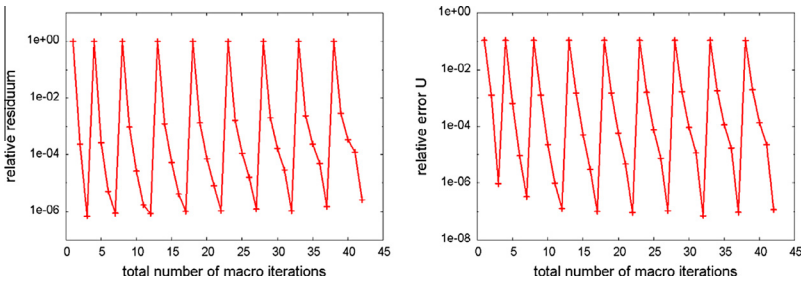

Fig. 7. Relative residuum (left) and relative error of the solution $\|\Delta \boldsymbol{U}\|/\|\boldsymbol{U}\|$ (right) of the macroscale over the total number of Newton iterations.

could be chosen. The polymer matrix of the RVE is modeled with the isotropic damage model and the behavior of the fibers is assumed to be linear elastic.

An exemplary micro field computed during the multiscale simulation is monitored in Fig. 9. At the right the relative error of the macroscopic solution field is plotted over the total number of macro iterations. Quadratic convergence can be observed clearly.

During the computation of this example approximately 20,000 unit cell calculations consisting each of 262,144 voxel cells had to be performed. The computational time of the entire problem which has not been parallelized yet (i.e. the RVE computations were performed sequentially) was around 240 h on a single CPU of a standard workstation. The computation of a single micro problem including the macroscopic load case and six homogenization load cases was distributed over five threads and took on average approximately 40 s. The last value strongly depends on the nonlinearity of the micro problem.

4.3. Multiscale simulation L-profile

In the last example a very challenging macro structural example is demonstrated. An L-shaped structure is discretized with 1650 tetrahedral finite elements of which 93 in the most critical region are coupled to the short fiber reinforced RVE structure already used in the example above, see Fig. 10. Linear elastic material behavior is assigned to the remaining area of the macroscopic structure. The polymer matrix of the RVE is modeled by the isotropic damage model and the behavior of the fibers is assumed to be linear elastic.

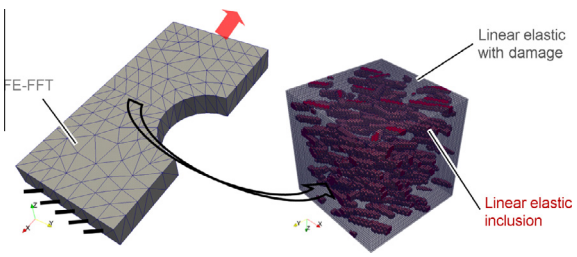

Fig. 8. Fully coupled micro–macro computation of a strip with a hole (left) and a short fiber reinforced composite structure (right).

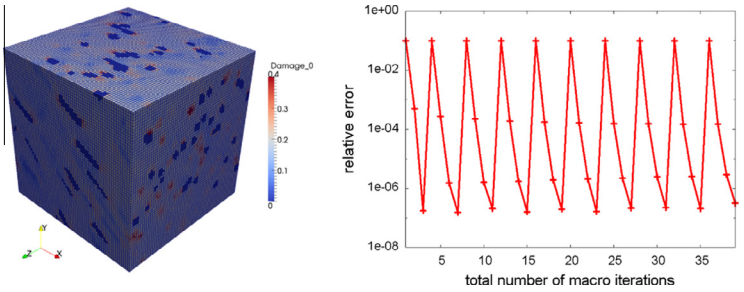

Fig. 9. Exemplary micro damage field (left) and relative error of the solution $\|\Delta \boldsymbol{U}\|/\|\boldsymbol{U}\|$ of the macroscale over the total number of Newton iterations (right).

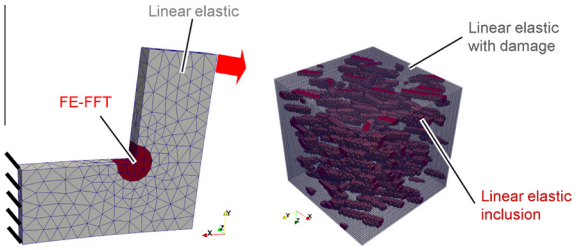

Fig. 10. Coupled micro–macro computation of an L-profile (left) and a short fiber reinforced composite structure (right). The constitutive equation of the macroscale is replaced in the most critical regions by a multiscale approach.

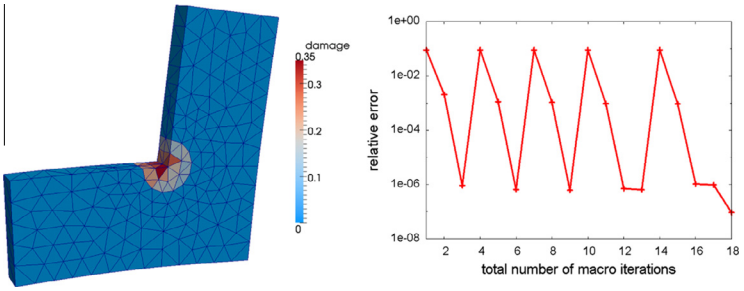

Fig. 11. Macroscopic damage field in the vertex of the L-profile (left) and relative error of the solution $\|\Delta \boldsymbol{U}\|/\|\boldsymbol{U}\|$ of the macroscale over the total number of Newton iterations (right).

The damage distribution of the L-profile computed during the multiscale simulation is illustrated in Fig. 11. At the right the relative error of the macroscopic solution field is plotted over the total number of macro iterations. The simulation was stopped when the relative error of the macro solution $\boldsymbol{U}$ falls below a value of 10^{-6}.

The simulation was aborted at the fifth load step due to convergence problems, because the microscale started to localize at this point. The CPU time amounts to approximately 17 h on a standard workstation.

5. Conclusions

In this work we proposed an efficient multiscale approach similar to FE^2 to investigate progressive damage behavior of composite materials. An alternative microscopic BVP formulation was chosen, which is obtained by rewriting a periodic micro BVP known from ordinary elasticity problems in an integral formulation of a so called Lippmann–Schwinger type. The efficiency of the numerical method which stems from an efficient fast Fourier transformation enables to compute larger and more realistic micro structures. Nonlinear material effects caused by microscopic physical effects were modeled on a finer length scale and used to predict the macroscopic damage behavior. Besides the isotropic elastic damage model used in this work basically any arbitrary (anisotropic) kind of material model could be implemented, like e.g including plasticity

effects, which is a subject of our current work. Within this method the exact physical response of arbitrary microstructures under different loading conditions is obtained. The convergence of the microscale problem is demonstrated on a unit cell computation, which contains a single spherical inclusion.

For the investigation of the macroscopic damage behavior the microscopic model is extended to a multiscale framework. Therefore two scales are related to each other by a procedure similar to the FE^2 approach. Thus, the constitutive equation on the macroscale which is discretized by the finite element method is replaced by the microscopic BVP described above. In this contribution the scale coupling technique and the computation of the macroscopic tangent by the perturbation procedure were described. The onset of localization on the macroscale is studied by an acoustic analysis of the homogenized tangent operator. Furthermore, in some numerical examples the convergence behavior of the macroscopic Newton algorithm is investigated. Quadratic convergence for all load steps was observed.

References

[1] J. Aboudi, Micromechanical analysis of composites by the method of cells-update, Applied Mechanics Reviews 49 (1996) 83.
[2] T. Belytschko, S. Loehnert, J.-H. Song, Multiscale aggregating discontinuities: a method for circumventing loss of material stability, International Journal for Numerical Methods in Engineering 73 (6) (2008) 869–894.
[3] T. Belytschko, J. Song, Coarse-graining of multiscale crack propagation, International journal for numerical methods in engineering 81 (5) (2010) 537–563.
[4] S. Brisard, L. Dormieux, FFT-based methods for the mechanics of composites: a general variational framework, Computational Materials Science 49 (3) (2010) 663–671.
[5] P. Castañeda, The effective mechanical properties of nonlinear isotropic composites, Journal of the Mechanics and Physics of Solids 39 (1) (1991) 45–71.
[6] P. Castañeda, Exact second-order estimates for the effective mechanical properties of nonlinear composite materials, Journal of the Mechanics and Physics of Solids 44 (6) (1996) 827–862.
[7] P. Castañeda, P. Suquet, Nonlinear composites, Advances in Applied Mechanics 34 (1997) 171–302.
[8] J. Chaboche, S. Kruch, J. Maire, T. Pottier, Towards a micromechanics based inelastic and damage modeling of composites, International Journal of Plasticity 17 (4) (2001) 411–439.
[9] E. Coenen, V. Kouznetsova, M. Geers, Multi-scale continuous–discontinuous framework for computational-homogenization-localization, Journal of Mechanics Physics of Solids 60 (2012) 1486–1507.
[10] R. Cuntze, Efficient 3D and 2D failure conditions for UD laminae and their application within the verification of the laminate design, Composites Science and Technology 66 (7) (2006) 1081–1096.
[11] R. De Borst, L. Sluys, H.-B. Muhlhaus, J. Pamin, Fundamental issues in finite element analyses of localization of deformation, Engineering Computations 10 (2) (1993) 99–121.
[12] J.E. Dennis, R.B. Schnabel, Numerical Methods for Unconstrained Optimization and Nonlinear Equations, vol. 16, Society for Industrial and Applied Mathematics, 1987.
[13] G.J. Dvorak, Transformation field analysis of inelastic composite materials, Proceedings of the Royal Society of London. Series A: Mathematical and Physical Sciences 437 (1900) (1992) 311–327.
[14] J.D. Eshelby, The determination of the elastic field of an ellipsoidal inclusion, and related problems, Proceedings of the Royal Society of London. Series A. Mathematical and Physical Sciences 241 (1226) (1957) 376–396.
[15] D. Eyre, G. Milton, A fast numerical scheme for computing the response of composites using grid refinement, EPJ Applied Physics 6 (1999) 41–48.
[16] F. Feyel, J. Chaboche, FE2 multiscale approach for modelling the elastoviscoplastic behaviour of long fibre SiC/Ti composite materials, Computer Methods in Applied Mechanics and Engineering 183 (3) (2000) 309–330.
[17] J. Fish, K. Shek, M. Pandheeradi, M.S. Shephard, Computational plasticity for composite structures based on mathematical homogenization: theory and practice, Computer Methods in Applied Mechanics and Engineering 148 (1) (1997) 53–73.
[18] Z. Hashin, S. Shtrikman, A variational approach to the theory of the elastic behaviour of multiphase materials, Journal of the Mechanics and Physics of Solids 11 (2) (1963) 127–140.
[19] R. Hill, Acceleration waves in solids, Journal of the Mechanics and Physics of Solids 10 (1) (1962) 1–16.
[20] R. Hill, Elastic properties of reinforced solids: some theoretical principles, Journal of the Mechanics and Physics of Solids 11 (5) (1963) 357–372.
[21] R. Hill, A self-consistent mechanics of composite materials, Journal of the Mechanics and Physics of Solids 13 (4) (1965) 213–222.
[22] R. Hill, The mathematical theory of plasticity, Vol. 11, Oxford university press, 1998.
[23] M. Kabel, H. Andrä, Numerical bounds of effective elastic moduli, Berichte des Fraunhofer ITWM 224 (1) (2012) 1–13.
[24] L. Kachanov, Introduction to Continuum Damage Mechanics, vol. 10, Springer, 1986.
[25] P. Kanouté, D. Boso, J. Chaboche, B. Schrefler, Multiscale methods for composites: a review, Archives of Computational Methods in Engineering 16 (1) (2009) 31–75.
[26] V. Kouznetsova, W. Brekelmans, F. Baaijens, An approach to micro–macro modeling of heterogeneous materials, Computational Mechanics 27 (1) (2001) 37–48.
[27] E. Kröner, Bounds for effective elastic moduli of disordered materials, Journal of the Mechanics and Physics of Solids 25 (2) (1977) 137–155.
[28] E. Kuhl, Numerische Modelle für kohäsive Reibungsmaterialien, Inst. f. Baustatik d. Univ, Stuttgart, 2000.
[29] J. Lemaitre, R. Desmorat, Engineering Damage Mechanics: Ductile, Creep, Fatigue and Brittle Failures, Springer, 2005.
[30] B. Lippmann, J. Schwinger, Variational principles for scattering processes. I, Physical Review 79 (3) (1950) 469.
[31] P. Maimí, P. Camanho, J. Mayugo, C. Dávila, A continuum damage model for composite laminates: Part I. Constitutive model, Mechanics of Materials 39 (10) (2007) 897–908.
[32] J. Mazars, G. Pijaudier-Cabot, Continuum damage theory-application to concrete, Journal of Engineering Mechanics 115 (2) (1989) 345–365.
[33] J. Michel, H. Moulinec, P. Suquet, Effective properties of composite materials with periodic microstructure: a computational approach, Computer Methods in Applied Mechanics and Engineering 172 (1) (1999) 109–143.
[34] J. Michel, H. Moulinec, P. Suquet, A computational method based on augmented Lagrangians and fast fourier transforms for composites with high contrast, CMES (Computer Modelling in Engineering & Sciences) 1 (2) (2000) 79–88.
[35] J. Michel, H. Moulinec, P. Suquet, A computational scheme for linear and non-linear composites with arbitrary phase contrast, International Journal for Numerical Methods in Engineering 52 (1–2) (2001) 139–160.
[36] J.-C. Michel, P. Suquet, Nonuniform transformation field analysis, International Journal of Solids and Structures 40 (25) (2003) 6937–6955.
[37] C. Miehe, Numerical computation of algorithmic (consistent) tangent moduli in large-strain computational inelasticity, Computer Methods in Applied Mechanics and Engineering 134 (3) (1996) 223–240.
[38] C. Miehe, A. Koch, Computational micro-to-macro transitions of discretized microstructures undergoing small strains, Archive of Applied Mechanics 72 (4) (2002) 300–317.
[39] T. Mori, K. Tanaka, Average stress in matrix and average elastic energy of materials with misfitting inclusions, Acta Metallurgica 21 (5) (1973) 571–574.

[40] H. Moulinec, P. Suquet, A fast numerical method for computing the linear and nonlinear mechanical properties of composites, Comptes rendus de l'Académie des sciences. Série II, Mécanique, Physique, Chimie, Astronomie 318 (11) (1994) 1417–1423.
[41] H. Moulinec, P. Suquet, A numerical method for computing the overall response of nonlinear composites with complex microstructure, Computer Methods in Applied Mechanics and Engineering 157 (1) (1998) 69–94.
[42] T. Mura, Micromechanics of Defects in Solids, vol. 3, Kluwer Academic Pub., 1987.
[43] S. Nemat-Nasser, M. Hori, Micromechanics: Overall Properties of Heterogeneous Materials, vol. 2, Elsevier Amsterdam, 1999.
[44] S. Pinho, R. Darvizeh, P. Robinson, C. Schuecker, P. Camanho, Material and structural response of polymer-matrix fibre-reinforced composites, Journal of Composite Materials 46 (19–20) (2012) 2313–2341.
[45] A. Puck, H. Schürmann, Failure analysis of FRP laminates by means of physically based phenomenological models, Composites Science and Technology 58 (7) (1998) 1045–1067.
[46] J. Rice, J. Rudnicki, A note on some features of the theory of localization of deformation, International Journal of Solids and Structures 16 (7) (1980) 597–605.
[47] J. Simo, J. Ju, Strain-and stress-based continuum damage models. I. Formulation, International Journal of Solids and Structures 23 (7) (1987) 821–840.
[48] R. Smit, W. Brekelmans, H. Meijer, Prediction of the mechanical behavior of nonlinear heterogeneous systems by multi-level finite element modeling, Computer Methods in Applied Mechanics and Engineering 155 (1) (1998) 181–192.
[49] I. Temizer, P. Wriggers, On the computation of the macroscopic tangent for multiscale volumetric homogenization problems, Computer Methods in Applied Mechanics and Engineering 198 (3) (2008) 495–510.
[50] S. Tsai, E. Wu, A general theory of strength for anisotropic materials, Journal of Composite Materials 5 (1) (1971) 58–80.
[51] E. Weinan, B. Engquist, X. Li, W. Ren, E. Vanden-Eijnden, Heterogeneous multiscale methods: a review, Communications in Computational Physics 2 (3) (2007) 367–450.
[52] R. Zeller, P. Dederichs, Elastic constants of polycrystals, Physica Status Solidi (b) 55 (2) (1973) 831–842.
[53] T.I. Zohdi, P. Wriggers, An Introduction to Computational Micromechanics, vol. 20, Springer Science+Business Media, 2008.
[54] C. Linder, R. Arun, A strong discontinuity approach on multiple levels to model solids at failure. Computer Methods in Applied Mechanics and Engineering (2012).
[55] C. Linder, Z. Xiaoxuan, A marching cubes based failure surface propagation concept for three-dimensional finite elements with non-planar embedded strong discontinuities of higher-order kinematics. International Journal for Numerical Methods in Engineering 96.6 (2013) 339–372.